Testing nonlocal nucleon-nucleon interactions in four-nucleon systems

Rimantas Lazauskas
CEA/DAM/DPTA Service de Physique Nucléaire, BP 12, F-91680 Bruyères-le-Châtel, France

Jaume Carbonell
Laboratoire de Physique Subatomique et de Cosmologie, 53 Avenue des Martyrs, 38026 Grenoble Cedex, France
(Received 18 June 2004; published 19 October 2004)

The Faddeev-Yakubovski equations are solved in configuration space for the α-particle and $n-{}^3$H continuum states. We test the ability of nonlocal nucleon-nucleon interaction models to describe $3N$ and $4N$ systems.

DOI: 10.1103/PhysRevC.70.044002 PACS number(s): 21.45.+v, 11.80.Jy, 25.40.−h, 25.10.+s

I. INTRODUCTION

In a fundamental description of nucleon-nucleon (*NN*) interaction, the existence of the nucleon internal structure cannot be ignored. The standard *NN* potentials are actually effective tools aiming to mimic a much more complicated interaction process, of which it is not even clear that it could be reduced to a potential problem. The *NN* system can be rigorously described only when starting from the underlying QCD theory for the nucleon constituents: quarks and gluons. This is, however, a very difficult task, which is just becoming accessible in lattice calculations [1–3], and that will be in any case limited for a long time to the two-nucleon system. In any attempt to describe the nuclear structure, one is thus obliged to rely on more or less phenomenological models.

Since the nucleon size is comparable to the strong interaction range, the effects of its internal structure are expected to be considerable. In particular the *NN* interaction should be nonlocal, at least for small internucleon distances. In addition, we have no reason to believe that nuclear interaction is additive as the Coulomb one: the interaction between two nucleons may not be independent of the presence of a third one in their vicinity. Finally the interplay of nucleon confinement and relatively large kinetic energies can generate—e.g., via virtual nucleon excitations—a rather strong energy dependence in the interaction. Despite numerous studies devoted to this subject, we still do not have a clear understanding of the relative importance of these effects in *NN* force, specially concerning their influence on experimentally measurable quantities.

This work investigates the consequences of using nonlocal *NN* forces in describing the $A=3$ and $A=4$ nuclear systems. The locality of *NN* force, assumed in some of the so-called realistic models [4,5], is due more to numerical convenience than to convincing physical arguments. The two-nucleon experimental data, since they contain only on-shell physics, are successfully reproduced without including any energy dependence or nonlocality in the *NN* force. However, they all suffer from the underbinding problem, i.e., two-nucleon interaction alone fails to reproduce the nuclear binding energies, starting already from the simplest $A=3$ nuclei. Figure 1 shows the relative differences between experimental and theoretical binding energies for He isotopes obtained with AV18 potential [4,6,7]. These differences increase with the mass number A and vary from $\sim$0.7 MeV in ^{3}He to $\sim$10 MeV in the case of ^{10}He.

The inclusion of nonlocal terms—as in Nijm 93 and Nijm I potentials [5]—does not remove this discrepancy [8,9]. If in some cases, as in CD-Bonn [10] or in chiral models [11–13], they considerably improve $3N$ and $4N$ binding energies, the improvement is still not sufficient to reproduce the experimental values. This underbinding is rather easily removed by means of three-nucleon forces (3NF). The existence of such forces is doubtless, but their strength depends on the *NN* partner in use and is determined only by fitting requirements.

However, the use of 3NF, to some extent, can be just a matter of taste. It has been shown in Refs. [14,15] that two different, but phase-equivalent, two-body interactions are related by a unitary, nonlocal, transformation. One thus could expect that a substantial part of $3N$ and multinucleon forces could also be absorbed by nonlocal terms. A considerable simplification would result if the bulk of experimental data could be described by only using two-body nonlocal interaction. In fact, the unique aim of any phenomenological model is to provide a satisfactory description of the experimental observables, but it is worth reaching this aim by using the simplest possible approach.

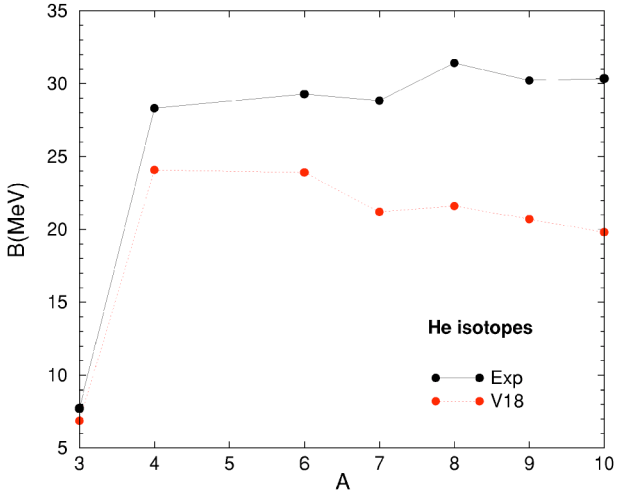

FIG. 1. (Color online) Comparison between the experimental and theoretical calculations with AV18 interaction in He isotopes. Results are taken from Refs. [6,7].

Already there exist calculations reproducing the triton binding energy without making explicit use of 3NF. The first one was obtained by Stadler and Gross [16] using a relativistic equation and benefiting from some additional freedom in the off-shell vertex form factors. The complexity in using relativistic equations, however, makes their extension to larger nuclear systems, or even to 3*N* scattering, difficult.

A very promising result, which takes profit from nonlocality in nonrelativistic nuclear models, has been obtained by Doleschall and collaborators [17–23]. In this series of papers, purely phenomenological nonlocal *NN* forces have been constructed, which were able to overcome the lack of binding energy in three-nucleon systems, namely ^{3}H and ^{3}He, without explicitly using 3NF and still reproducing 2*N* observables. The striking success of these models is closely related to the presence of small deuteron *D*-state probability, comparatively to local *NN* interaction, a difference which does not contradict the phenomenology and which follows from using two equivalent representations of the one and the same physical object [24]. In fact, nonlocality of the Doleschall potential softens the short range repulsion of local *NN* models and can simulate part of the effects due to the 6-quark structures as well as quark exchange between nucleons inside the nucleus. Local realistic interaction models, maybe with the exception of the Moscow [25] potential, artificially prohibits such effects by imposing a very strong short-range repulsion.

Our work is an extension to the $A=4$ nuclei of the Doleschall pioneering studies. In particular, we would like to check whether such nonlocal interaction models remain successful or not when applied to the more complicated 4*N* systems. We will first provide results for ^{4}He ground state and then extend the calculations to the $n-^3$H scattering. This system possesses a resonance at $E_{\mathrm{c.m.}}\approx 3$ MeV, exhibiting different dynamical properties from those of bound states and testifying to a failure of the conventional *NN*+3NF interaction models [26].

II. THEORETICAL TREATMENT

A. FY Equations

We describe the 4*N* system by using Faddeev-Yakubovski (FY) equations in configuration space [27–29]. Even though the major goal of FY formalism is a mathematically rigorous description of the continuum states, it turns out as well to be advantageous when dealing with a bound state problem. The advantage lies in the natural decomposition of the wave function in terms of the so-called Faddeev-Yakubovski components (FYC) which make use of the system's symmetry properties. These amplitudes have a simpler structure than the wave function itself and are therefore easier to handle numerically. Four-particle systems require the use of two types of FYC, namely *K* and *H*. Asymptotes of components *K* incorporate 3+1 (see Fig. 2) channels, while components *H* contain asymptotes of 2+2 ones (see Fig. 2). By permuting the particles one can construct twelve different components of the type *K* and six components of the type *H*. The total wave function is simply a sum of these 18 FYC.

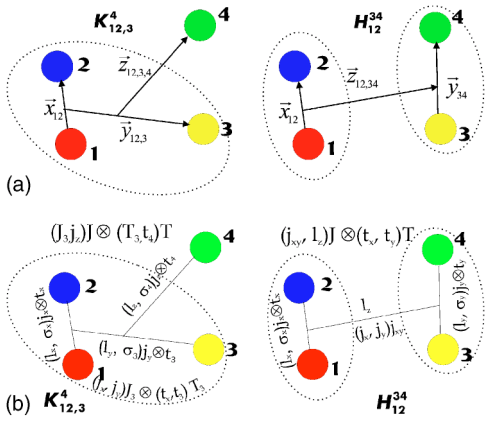

FIG. 2. (Color online) (a) FY components *K* and *H*. Asymptotically, as $z\rightarrow\infty$, components *K* describe 3+1 particle channels, whereas components *H* contain asymptotic states of 2+2 channels. (b) The *j*-*j* coupling schemes used when developing FYC *K* and *H* into a partial wave basis.

In the theoretical treatment of the problem we use the isospin formalism, i.e., we consider protons and neutrons as being degenerate states of the same particle—nucleon. For a system of identical particles, the FYC are not completely independent, being related by several straightforward symmetry relations. All the 18 FYC can be obtained by the action of the permutation operators on two of them, arbitrarily chosen, provided one is of type *K* and the other of type *H*. We have chosen $K\equiv\Psi^4_{12,3}$ and $H\equiv\Psi^{34}_{12}$. The four-body problem is solved by determining these two components, which satisfy the system of differential equations [29]:

$$(E-H_0-V)K=V(P^++P^-)[(1+Q)K+H],$$

$$(E-H_0-V)H=V_{12}\tilde{P}[(1+Q)K+H]. \tag{1}$$

P^+, P^-, $\tilde{P}$, and Q are the permutation operators:

$$P^+=(P^-)^{-1}=P_{23}P_{12},$$

$$Q=\varepsilon P_{34},$$

$$\tilde{P}=P_{13}P_{24}=P_{24}P_{13}.$$

Employing the operators defined above, the system's wave function is given by

$$\Psi=[1+(1+P^++P^-)Q](1+P^++P^-)K$$
$$+(1+P^++P^-)(1+\tilde{P})H. \tag{2}$$

Components *K* and *H* are functions in configuration space, and depend also on the internal degrees of freedom of the individual particles (spins and isospins). The configuration space is provided by the position of the different particles, which we describe by using reduced relative coordinates. These coordinates differ from Jacobi coordinates usually employed in classical mechanics by factors depending on the particle masses. Use of such coordinates has several big advantages: first, center of mass motion can be easily separated, then transition between two bases is equivalent to

orthogonal transformation in $R^{3(N-1)}$ space; finally, kinetic energy operator in this basis reduces to a multidimensional Laplace operator in corresponding subspaces. Two principally different sets of reduced relative coordinates can be defined. One is associated with the components $K \equiv \Psi^{l}_{ij,k}$:

$$\vec{x}_{ij} = \sqrt{2\frac{m_i m_j}{m_i + m_j}}(\vec{r}_j - \vec{r}_i),$$

$$\vec{y}_{ij,k} = \sqrt{2\frac{(m_i + m_j)m_k}{m_i + m_j + m_k}}\left(\vec{r}_k - \frac{m_i\vec{r}_i + m_j\vec{r}_j}{m_i + m_j}\right),$$

$$\vec{z}_{ijk,l} = \sqrt{2\frac{(m_i + m_j + m_k)m_l}{m_i + m_j + m_k + m_l}}\left(\vec{r}_l - \frac{m_i\vec{r}_i + m_j\vec{r}_j + m_k\vec{r}_k}{m_i + m_j + m_k}\right), \tag{3}$$

where m_ℓ and $\vec{r}_\ell$ are, respectively, the mass and the position of the ℓth particle. The coordinate set associated with the components $H \equiv \Psi^{kl}_{ij}$ is defined by

$$\vec{x}_{ij} = \sqrt{2\frac{m_i m_j}{m_i + m_j}}(\vec{r}_j - \vec{r}_i),$$

$$\vec{y}_{kl} = \sqrt{2\frac{m_k m_l}{m_k + m_l}}(\vec{r}_l - \vec{r}_k),$$

$$\vec{z}_{ij,kl} = \sqrt{2\frac{(m_i + m_j)(m_k + m_l)}{m_i + m_j + m_k + m_l}}\left(\frac{m_k\vec{r}_k + m_l\vec{r}_l}{m_k + m_l} - \frac{m_i\vec{r}_i + m_j\vec{r}_j}{m_i + m_j}\right). \tag{4}$$

The functions K and H are expanded on the basis of partial angular momentum, spin and isospin variables, according to the equation

$$\Phi_i(\vec{x}_i,\vec{y}_i,\vec{z}_i) = \sum_\alpha \frac{\mathcal{F}^\alpha_i(x_i,y_i,z_i)}{x_i y_i z_i} Y^\alpha_i(\hat{x}_i,\hat{y}_i,\hat{z}_i). \tag{5}$$

Here $Y^\alpha_i(\hat{x}_i,\hat{y}_i,\hat{z}_i)$ generalize tripolar harmonics containing spin, isospin, and angular momentum variables. Functions $\mathcal{F}^\alpha_i(x_i,y_i,z_i)$ are so-called partial amplitudes, being continuous in radial variables x, y, and z. The label α represents the set of intermediate quantum numbers defined in coupling scheme; it includes as well the specification for the type of FY component (K or H). We have used j-j couplings, represented in Fig. 2(b), and expressed by

$$[\{(t_i t_j)_{t_x} t_k\}_{T_3} t_l]_{\mathcal{T}} \langle \{[l_x(s_i s_j)_{\sigma_x}]_{j_x}[l_y s_k]_{j_y}\}_{J_3}[l_z s_l]_{j_z}\rangle_{\mathcal{J}^\pi} \tag{6}$$

for components of K-type and

$$[(t_i t_j)_{t_x}(t_k t_l)_{t_y}]_{\mathcal{T}} \langle \{[l_x(s_i s_j)_{\sigma_x}]_{j_x}[l_y(s_k s_l)_{\sigma_y}]_{j_y}\}_{j_{xy}} l_z\rangle_{\mathcal{J}^\pi} \tag{7}$$

for the H-type components. Here s_i and t_i are the spin and isospin quantum numbers of the individual particles and $(\mathcal{J}^\pi,\mathcal{T})$ are, respectively, the total angular momentum, parity, and isospin of the four-body system. Each amplitude $\mathcal{F}^\alpha_i(x_i,y_i,z_i)$ is thus labeled by the set of 12 quantum numbers α. The symmetry properties of the wave function with respect to the exchange of two particles impose additional constraints. One should have $(-1)^{l_x+\sigma_x+t_x}=\varepsilon$ for the amplitudes derived from any type of components (K or H), while for H-type amplitudes additional constraint $(-1)^{l_y+\sigma_y+t_y}=\varepsilon$ is valid as well. Since we deal with nucleons (i.e., fermions), Pauli factor ε is equal to -1. The total parity π is given by $(-1)^{l_x+l_y+l_z}$, independently of the coupling scheme in use.

By projecting each of Eqs. (1) on its natural configuration space basis, one obtains a system of coupled integrodifferential equations. In general one has an infinite number of coupled equations. Note that, contrary to the $3N$ problem, the number of partial FY amplitudes is infinite even when the pair interaction is restricted to a finite number of partial waves. This divergence comes from the existence of additional degree of freedom l_z in the expansion of the K-type components. Therefore we are obliged to make additional truncations in numerical calculations by taking into account only the most relevant amplitudes.

B. Boundary conditions

Equations (1) are not complete and should be complemented with the appropriate boundary conditions. Boundary conditions can be written in the Dirichlet form. First FY amplitudes, for bound as well as for scattering states, satisfy the regularity conditions:

$$\mathcal{F}^\alpha_i(0,y_i,z_i) = \mathcal{F}^\alpha_i(x_i,0,z_i) = \mathcal{F}^\alpha_i(x_i,y_i,0) = 0. \tag{8}$$

For the bound state problem, the wave function is exponentially decreasing and therefore the regularity conditions can be completed by forcing the amplitudes $\mathcal{F}^\alpha_i$ to vanish at the borders of the hypercube $[0,X_{\max}]\times[0,Y_{\max}]\times[0,Z_{\max}]$, i.e.,

$$\mathcal{F}^\alpha_i(X_{\max},y_i,z_i) = \mathcal{F}^\alpha_i(x_i,Y_{\max},z_i) = \mathcal{F}^\alpha_i(x_i,y_i,Z_{\max}) = 0. \tag{9}$$

For the elastic scattering problem the boundary conditions are implemented by imposing at large values of z the asymptotic behavior of the solution. In case of $N+NNN$ elastic scattering we impose at $Z_{\max}$ the solution of the $3N$ problem for all the quantum numbers, corresponding to the open channel α_a:

$$\mathcal{F}^{\alpha_a}_i(x_i,y_i,Z_{\max}) = f^{\alpha_a}_i(x_i,y_i). \tag{10}$$

Functions $f^{\alpha_a}_i(x_i,y_i)$ are the Faddeev amplitudes obtained after solving the corresponding $3N$ bound state problem. Indeed, below the first inelastic threshold, at large values of z, the solution of Eqs. (1) factorizes into a bound state solution of $3N$ Faddeev equations and a plane wave propagating in the z direction with the momentum $k_{\alpha_a} = \sqrt{(m/\hbar^2)(E_{\text{c.m.}} - E_{3N})}$. One has

$$\mathcal{F}^{\alpha_a}_i(x_i,y_i,z_i) \sim f^{\alpha_a}_i(x_i,y_i)[\hat{j}_{l_z}(k_{\alpha_a} z_i) + \tan(\delta)\hat{n}_{l_z}(k_{\alpha_a} z_i)].$$

There are two different ways to obtain the scattering observables. The easier one is to extract the scattering phases from the tail of the solution, namely taking the logarithmic derivative of the open channel's K amplitude α_a in the asymptotic region:

TABLE I. ^{3}H and ^{3}He binding energies (in MeV) calculated with various versions of nonlocal Doleschall potentials and with the AV18+UIX model. Results are compared to experimental values and previous calculations. ΔB denotes the difference between ^{3}H and ^{3}He binding energies.

	^{3}H		^{3}He		ΔB	
	This work	Other	This work	Other	This work	Other
INOY96	8.556		7.882		0.674	
INOY03	8.497	8.482 [22]	7.734	7.718 [22]	0.763	0.764
INOY04	8.476		7.711		0.765	
INOY04′	8.464	8.481 [23]	7.704	7.718 [23]	0.760	0.763
AV18	7.616	7.618(2) [32]	6.914	6.917(2) [32]	0.699	
AV18+UIX	8.473	8.474(4) [32]	7.739	7.742(4) [32]	0.734	
Expt.	8.482		7.718		0.764	

$$\tan\delta = \frac{k_{\alpha_a}\hat{j}_l'(k_{\alpha_a}z_i) - \dfrac{\partial_{z_i}\mathcal{F}_i^{\alpha_a}(x_i,y_i,z_i)}{\mathcal{F}_i^{\alpha_a}(x_i,y_i,z_i)}\hat{j}_l(k_{\alpha_a}z_i)}{\dfrac{\partial_{z_i}\mathcal{F}_i^{\alpha_a}(x_i,y_i,z_i)}{\mathcal{F}_i^{\alpha_a}(x_i,y_i,z_i)}\hat{n}_l(k_{\alpha_a}z_i) - k_{\alpha_a}\hat{n}_l'(k_{\alpha_a}z_i)}. \quad (11)$$

This result can be independently verified by using integral representation of the phase shifts

$$\sin\delta = -\frac{m}{\hbar^2}\int \Phi_{\alpha_a}^{(123)}(\vec{x}_i,\vec{y}_i)\hat{j}_l(k_{\alpha_a}z)(V_{14}+V_{24}+V_{34}) \times\Psi(\vec{x}_i,\vec{y}_i,\vec{z}_i)dV. \quad (12)$$

Here $\Phi_{\alpha_a}^{(123)}(\vec{x}_i,\vec{y}_i)$ is a $3N$ bound state wave function composed by particles (1,2,3). This wave function is considered to be normalized to unity. Asymptotes of the wave function $\Psi(\vec{x}_i,\vec{y}_i,\vec{z}_i)$ are considered to have the same normalization as $\Phi_{\alpha_a}^{(123)}(\vec{x}_i,\vec{y}_i)$, i.e., they tend to

$$\Psi(\vec{x}_i,\vec{y}_i,\vec{z}_i) = \Phi_{\alpha_a}^{(123)}(\vec{x}_i,\vec{y}_i)[\hat{j}_{l_z}(k_{\alpha_a}z_i) + \tan(\delta)\hat{n}_{l_z}(k_{\alpha_a}z_i)]. \quad (13)$$

A detailed discussion on these technical aspects can be found in Refs. [26,30].

C. Numerical solution

In order to solve the set of integrodifferential equations—obtained when projecting Eq. (1) in conjunction with the appropriate boundary conditions into partial wave basis—components $\mathcal{F}_i^\alpha$ are expanded in terms of piecewise Hermite spline basis:

$$\mathcal{F}_i^\alpha(x,y,z) = \sum c_{ijkl}^\alpha S_j(x)S_k(y)S_l(z).$$

In this way, integrodifferential equations are converted into an equivalent linear algebra problem with unknown spline expansion coefficients c_{ijkl}^α to determine. In the case of the bound state problem the eigenvalue-eigenvector problem is obtained:

$$Ac = EBc, \quad (14)$$

where A and B are square matrices, while E and c are, respectively, unknown eigenvalue(s) and its eigenvector(s) to determine. In the case of the elastic scattering problem, a system of linear algebra equations is obtained:

$$[A - E_{\text{c.m.}}B]c = b, \quad (15)$$

where b is an inhomogeneous term imposed by the boundary conditions, Eq.(10). Numerical methods used for solving these large scale $N\sim 10^7$ eigenvalue problems and linear systems are given in Ref. [26].

III. RESULTS AND DISCUSSION

We have used in our calculations four different Doleschall potentials derived in Refs. [17–23]. Hereafter, INOY96 denotes the SB+SDA version of the potential defined in Refs. [17,18]. It consists in short-range nonlocal potentials in $^1S_0$ and $^3SD_1$ partial waves continued with a local Yukawa tail outside $R=4$ fm. The other partial waves are taken from AV18. INOY03 denotes the IS version considered in Ref. [22]. It is an updated version of INOY96, which has a smaller nonlocality range ($R=2$ fm) and provides a more accurate description of $2N$ observables. INOY04 and INOY04′ are the two most recent versions [23] having the same $^1S_0$ and $^3SD_1$ potentials as INOY03, completed with the newly defined nonlocal potentials in P and D waves. As in the preceding models, higher partial waves are also taken from AV18.

All the results have been obtained considering equal masses for neutrons and protons ($m_n=m_p=m$) with $\hbar^2/m = 41.47$ MeV fm^2. As mentioned in Sec. II A we have used isospin formalism, furthermore assuming the total isospin quantum number $\mathcal{T}$ to be conserved.

A. $3N$ system

We will start with the presentation of our results concerning $3N$ systems. Binding energies for ^{3}H and ^{3}He nuclei are summarized in Table I. In order to control our accuracy, we have included in this table the results of AV18 [4] with and

TABLE II. Expectation values of kinetic ($\langle T\rangle$) energies, rms radius ($R=\sqrt{\langle r^2\rangle}$), and proton radius r_p corresponding to the binding energies of Table I. The values of the potential energy have been separated into contributions coming from the nonlocal $\langle V_{nl}\rangle$ and local $\langle V_l\rangle$ terms of the potential. For the AV18+UIX model, $\langle V_{nl}\rangle$ denotes the contribution of 3NF to potential energy. For ^{3}He, the expectation values of Coulomb interaction have not been included.

	Model	$\langle T\rangle$ (MeV)	$-\langle V_l\rangle$ (MeV)	$-\langle V_{nl}\rangle$ (MeV)	R (fm)	r_p (fm)
^{3}H	INOY96	34.24	0.776	42.02	1.656	1.561
	INOY03	33.11	5.551	36.06	1.664	1.566
	INOY04	33.01	5.564	35.92	1.667	1.567
	INOY04′	32.97	5.547	35.89	1.668	1.568
	AV18	46.71	54.32	—	1.770	1.654
	AV18+UIX	51.28	58.69	1.140	1.684	1.584
	Expt.					1.60
^{3}He	INOY96	33.64	0.777	41.42	1.684	1.733
	INOY03	32.33	5.512	35.21	1.701	1.752
	INOY04	32.24	5.510	35.08	1.703	1.755
	INOY04′	32.20	5.525	35.05	1.704	1.756
	AV18	45.68	53.30	—	1.809	1.867
	AV18+UIX	50.22	57.60	1.095	1.716	1.767
	Expt.					1.77

without Urbana IX (UIX) three-nucleon force [31]. One can see that we are in close agreement with the benchmark calculations of Ref. [32]. Our results concerning nonlocal potentials are slightly different from those given in Refs. [22,23]. The small deviations ($\approx$15 keV) come from isospin breaking effects which were fully included in Doleschall calculations [33] while, as discussed in the above section, they were only approximately taken into account in ours. These isospin effects for AV18+UIX have also been evaluated in Ref. [32] and were found to be of about 5 keV, i.e., three times less than in nonlocal models. In any case, the small differences related to isospin approximation cannot overcast the main achievement of these nonlocal interactions: the ability to reproduce experimental 3N binding energies without three-nucleon force. One can also note from Table I that, while the binding energies obtained with AV18+UIX are in good agreement with the experimental data, the value of $\Delta B=B_{^3\mathrm{H}}-B_{^3\mathrm{He}}$is better reproduced by nonlocal models.

The analysis of the 3N binding energies is shown in Table II. One can see that the major contribution to binding is due to the nonlocal short-range interaction terms $\langle V_{nl}\rangle$. Contributions from the local part—coming either from the long-range Yukawa tail or from higher partial waves—are marginal in INOY96 model and remain less than 15% in the other ones.

Comparison between INOYs and AV18+UIX results is instructive. Both models provide similar energies and rms radii but they result from values of kinetic and potential energies that differ as much as $\sim$50%. The introduction of a nonlocal interaction reduces the short-range repulsion between nucleons and makes the potential well more shallow. Deuterons are already obtained with the same binding energy and size as for the AV18 model but their wave function does not have, at short distances, the sharp slope due to hard-core repulsion. On the other hand, the weaker $^3S_1$-$^3D_1$ coupling in nonlocal models generates a smaller contribution of the D state. All these effects reduce the average kinetic energy and favor stronger binding in the 3N system, which is more compact than the deuteron. If the average size of the 3N system between two models is only slightly different, the average kinetic energy of nucleons is sensibly smaller in the case of nonlocal interactions.

The relative contributions (algebraic values) of the most relevant V_{NN} partial waves to the ^{3}H potential energy are given in Table III. The column labeled "Others" denotes the contribution of all partial waves not listed in the table. One

TABLE III. Relative contributions of different V_{NN} partial waves to triton potential energy.

	$^3S_1$	$^1S_0$	$^3D_1$	$^3P_2$	$^3P_0$	$^1D_2$	$^3P_1$	$^1P_1$	$^3D_2$	$^3D_3$	Others
INOY96	57.94	29.24	12.78	0.1658	0.1506	0.05664	−0.3810	−0.04528	0.04939	0.01505	0.02518
INOY03	58.30	30.31	11.42	0.1350	0.1892	0.04260	−0.4214	−0.05317	0.06144	0.01634	0.02307
INOY04	58.35	30.33	11.38	0.1409	0.1579	0.04843	−0.4304	−0.05495	0.06303	0.06460	0.0113
INOY04′	58.40	30.36	11.37	0.1478	0.7854	0.05061	−0.4368	−0.05711	0.06527	0.04333	0.0089
AV18	45.00	25.30	28.97	0.4466	0.2272	0.1840	−0.3977	−0.03244	0.07952	0.08769	0.1290

TABLE IV. Neutron-deuteron (nd) scattering lengths (in fm) calculated using Doleschall potentials.

	$^2a_{nd}$(fm)	$^4a_{nd}$(fm)
INOY96	0.448	6.34
INOY03	0.523	6.34
INOY04	0.543	6.34
INOY04′	0.553	6.34
AV18	1.26	6.34
AV18+UIX	0.595	6.34
Expt.	0.65±0.04	6.35±0.02

can note the small role of P waves. It was noticed a long time ago that the triton binding energy basically depends on $^1S_0$ and $^3S_1$-$^3D_1$ NN interactions. Indeed, in absence of the tensor force, the $3N$ ground state would have $L=0$ and $S=\frac{1}{2}$ as conserved quantum numbers and in this case P waves would not contribute at all. The $^3S_1$-$^3D_1$ tensor coupling introduces an $L=2$ admixture in the wave function. The $L=1$ state appears only in the second order and contributes less than 0.1%. NN P waves start acting only in the second order as well, which explains their negligible contribution to $3N$ binding energy, as shown in Table III. The reduction of the tensor force is also sizable: $^3D_1$ waves' contributions are considerably smaller for Doleschall interactions than for AV18.

The calculated n-d scattering lengths are presented in Table IV. The quartet value (^4a), corresponding to the $J^\pi=3/2^+$ state, is independent of the interaction model in use, furthermore being in full agreement with the experimental one. This robustness is due to the strong Pauli repulsion, prohibiting two neutrons to get close to each other. It follows that only $^3S_1$-$^3D_1V_{np}$ waves are important in describing the $J^\pi=3/2^+$ state and still only through its well-controlled, long-range part. Therefore, this state does not contain any off-shell physics and can be successfully described by any potential model, provided it reproduces the $J^\pi=1^+$ np scattering observables.

The integral representation of the phase shifts, Eq. (12), is used to study the role of different V_{NN} partial waves. In Table V are given the relative contributions to this integral. Their sum, in algebraic values, is normalized to 100. Results for n-d doublet scattering length (^2a) are presented in the upper half of the table and the quartet ones in the lower part. It can be seen that for $J^\pi=3/2^+$, NN waves other than $^3S_1$ contribute by less than 0.1%, which confirms the statements above. The situation is different for ^2a, which results mainly from a cancellation between $^1S_0$ and $^3S_1$ and is more sensitive to higher NN partial waves, showing a deeper impact into the off-shell physics. Due to the smallness of ^2a, all the interaction effects have to be taken into account very accurately. In particular, its value is very sensitive to the electromagnetic (e.m.) interaction terms. The differences between INOY predictions and the experiment can therefore be caused by the absence of e.m. terms in these models. On the contrary e.m. corrections were properly included in AV18+UIX results. In any case the small discrepancy with data has no consequences in phenomenology, since ^2a is by one order of magnitude smaller than ^4a and its relative contribution to the scattering cross sections is negligible.

B. 4N system

Our results concerning the α-particle binding energy are displayed in Table VI. Two series of calculations were performed, including (upper half of the table) and neglecting (lower half) the Coulomb repulsion between protons. This latter interaction was provided by the Argonne group in their AV18 code [4] and takes into account proton finite size effects.

Calculations have been done by considering isospin averaged pair interaction, i.e.,

$$V_{t_1t_2}=P_{nn}(t_1,t_2)V_{nn}+P_{pp}(t_1,t_2)V_{pp}+P_{np}(t_1,t_2)V_{np},$$

where (t_1,t_2) are the isospin quantum numbers of FY amplitudes in Eq. (5). They, respectively, represent (t_x,T_3) for K-type amplitudes and (t_x,t_y) for H-type ones. P_{nn}, P_{pp}, and P_{np} are the probabilities of finding, respectively, nn, pp, and np pairs in a given isospin state. Note that, since the number of protons and neutrons in the α particle is equal, one has $P_{nn}(t_1,t_2)=P_{pp}(t_1,t_2)$.

As in $3N$ calculations, we have neglected isospin breaking effects, considering the α particle as a pure $\mathcal{T}=0$ state. Con-

TABLE V. Relative contributions of different NN interaction waves in n-d integral scattering lengths. The doublet value is in the upper half of the table and quartet in the lower half.

	$^3S_1$	$^1S_0$	$^3D_1$	$^3P_2$	$^3P_0$	$^1D_2$	$^3P_1$	$^1P_1$	$^3D_2$	$^3D_3$	Others
INOY96	−685.3	800.3	−20.14	2.664	−1.240	−5.097	−11.97	20.07	−0.7484	0.6967	0.7998
INOY03	−572.6	685.2	−16.73	1.955	0.2399	−4.523	−10.95	16.73	−0.6048	0.3972	0.8616
INOY04	−549.6	662.4	−16.28	1.997	−0.3862	−4.257	−10.31	15.66	−0.5025	0.3749	0.8932
INOY04′	−538.5	650.8	−15.92	2.127	−1.076	−4.167	−9.308	15.25	−0.4694	0.3563	0.8825
AV18	−195.5	293.5	−4.283	4.779	0.6261	−0.3768	−5.944	6.190	−0.3316	0.9574	0.3281
INOY96	100.1	−0.0297	0.0183	−0.2708	−0.5036	−0.1510	0.8177	0.0190	−0.1644	0.0076	0.0312
INOY03	100.0	−0.0288	0.0199	−0.2694	−0.4640	−0.1529	0.8180	0.0192	−0.1641	0.00742	0.0315
INOY04	100.1	−0.0283	0.0197	−0.2707	−0.4938	−0.1515	0.8343	0.0189	−0.1653	−0.0006	0.0480
INOY04′	99.98	−0.0279	0.0195	−0.2675	−0.4973	−0.1503	0.9043	0.0188	−0.1651	−0.0004	0.0479
AV18	100.1	−0.0400	0.0097	−0.2672	−0.4870	−0.2577	0.8081	0.0252	−0.1691	0.0096	0.0361

TABLE VI. Binding energy B (in MeV) and rms radius R (in fm) for the ^{4}He ground state obtained with Doleschall and AV18 +UIX potentials. The lower part contains Coulomb force. Energies presented in the two last lines of the table, respectively, for AV18 and AV18+UIX models have been taken from Refs. [8,34], whereas the rms radius is from Ref. [6].

Potential	$\langle T\rangle$	$-\langle V\rangle$	B	R
INOY96	72.80	103.8	31.00	1.353
INOY03	69.89	99.94	30.04	1.369
INOY04	69.49	99.41	29.91	1.372
INOY04′	69.46	99.36	29.88	1.372
AV18	98.69	123.6	24.95	1.511
Potential	$\langle T\rangle$	$-\langle V\rangle$	$-\langle E\rangle$	R
INOY96	72.45	102.7	30.19	1.358
INOY03	69.54	98.79	29.24	1.373
INOY04	69.14	98.62	29.11	1.377
INOY04′	69.11	98.19	29.09	1.376
AV18	97.77	122.1	24.22	1.516
	97.80	122.0	24.23[8,34]	
AV18+UIX	113.2	141.7	28.50[8,34]	1.44 [6]
Expt.			28.30	1.47

tributions of $\mathcal{T}=1$, 2 admixture were calculated for AV18 and AV18+UIX models in Ref. [8] and found to be as small as 10 keV. Results for the 3N system presented in the last section showed that Doleschall nonlocal models are more sensible to isospin breaking: they account for $\approx$15 keV in ^{3}H compared to $\approx$5 keV in AV18+UIX [32]. In any case, for the α particle these effects should not exceed some 50 keV and will not affect the physics discussed below. Notice also that Coulomb corrections obtained by nonlocal models exceed by 70 keV those obtained by AV18, due to the different rms radii they give.

As mentioned in Sec. II A, FY calculations have been performed in the j-j coupling scheme. The following truncations in the partial wave expansion of amplitudes were used: (i) V_{NN} waves are limited to $l_x\leqslant 3$ but always include tensor-coupled partners, i.e., involving the set $^1S_0$, $^3SD_1$, $^1P_1$, $^3P_0$, $^3PF_2$, $^3P_1$, $^1D_2$, $^3DG_3$, $^3D_2$, $^1F_3$, $^3FH_4$, $^3F_3$, and (ii) $l_x+l_y+l_z\leqslant 10$.

Convergence was studied as a function of $j_{yz}=\max(j_y,j_z)$ for K-like components and $j_{yz}=\max(j_y,l_z)$ for H-like components, starting with $j_{yz}\leqslant 1$. In Table VII we present the α-particle binding energy results for INOY04′ and AV18 models, respectively. The convergence is rather smooth, except when passing from $j_{yz}\leqslant 5$ to $j_{yz}\leqslant 6$. We think this is an artefact of our truncation procedure which keeps the basis set fixed in the x coordinate. Note that the agreement between our results for the AV18 potential and those given in Refs. [8,34] is very good. From the results displayed in Table VII, as well as from analogous convergence patterns seen in 3N calculations, we conclude that Doleschall potentials converge more rapidly than AV18. This is probably due to their weaker tensor force, resulting into

TABLE VII. Results of the α-particle binding energy (in MeV) for INOY04′ and AV18 models with V_{NN} interaction limited to $l_x\leqslant 3$ (see text) and partial wave basis limited to $l_x+l_y+l_z\leqslant 10$. The convergence was searched as a function of $j_{yz}=\max(j_y,j_z)$ for K-like components and $j_{yz}=\max(j_y,j_z)$ for H-like components. The last line, denoted by an asterisk, contains additional calculations with NN interaction waves up to $j_x\leqslant 6$ and $l_x+l_y+l_z\leqslant 12$.

j_{yz}	INOY04′	AV18
1	28.094	
2	28.661	
3	28.967	
4	28.971	23.897
5	28.974	23.920
6	29.084	24.233
7	29.085	24.226
*	29.085	24.223

wave functions with stronger spherical symmetry.

To our opinion the main conclusion of the results displayed in Table VI is the possibility offered by the INOY models to provide a satisfactory description of $A=4$ nuclei in terms of two-body forces alone, as it is already the case for $A=2$ and 3. One can argue that this agreement is not yet fully realized in their present version, for they all slightly overbind the experimental value: the most favorable version (INOY04′) still exceeds the ^{4}He binding energy by 0.79 MeV. One should, however, note that this result is obtained without adjusting any additional parameter with respect to $A=3$. On the other hand, the difference between INOY96 and INOY04′—due essentially to different parameterizations of their nonlocal short-range parts—is 1.1 MeV. It seems thus possible, by a finer tuning, to reach an even more precise description of $A=4$ in a next generation of potentials. If they are not contradicted by other aspects of the phenomenology, INOY models offer an alternative description permitting to avoid three-nucleon forces.

Results of Table VI have been gathered in a Tjon plot—see Fig. 3—which displays the correlation between ^{3}H and ^{4}He binding energies for various NN potentials. One can see that, due to the small overbinding of the α particle, INOY results (diamond symbols) are outside the line formed by realistic local model predictions and, except for INOY96, are almost superimposed to CD Bonn+Tucson-Melbourne (TM) value.

INOY03, INOY04, and INOY04′ models, which differ in their P-wave structure, give very close results, while INOY96, which has a different nonlocal S-wave structure, falls out further apart. This indicates that the S waves are the key point in binding α particles, and in order to improve the agreement with the experimental value a better tuning in the $^3S_1-{}^3D_1$ and $^1S_0$ could be helpful.

Proton rms radii predicted by INOY potentials deserve some comments. One can see already in 3N systems (see Table II) that they are slightly smaller than the experimental ones. For α particles we have only calculated average rms of nucleons, without making a distinction between neutrons and

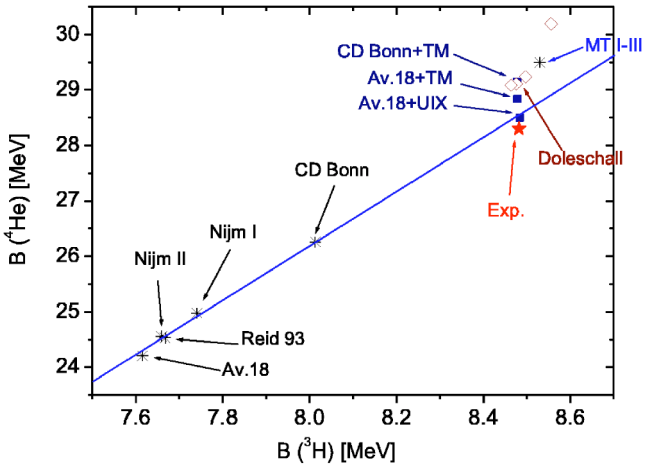

FIG. 3. (Color online) Tjon line for the local and nonlocal *NN* potentials.

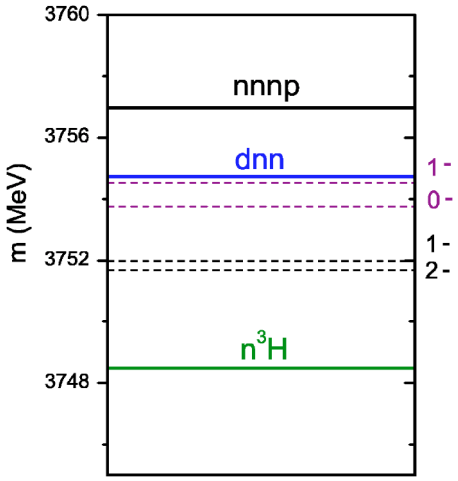

FIG. 4. (Color online) Negative-parity resonance above the $n+t$ threshold.

protons. The real value of protons rms should be slightly larger. However, since Coulomb interaction has a very small effect on the α-particle wave function (rms radii calculated by taking Coulomb interaction into and without account differ only in fourth digit), this value cannot differ by more than 0.5%. One can, therefore, see that protons rms provided by the INOY model are already by 6% smaller than the experimental one, compared to 1–2 % in the 3*N* complex. This fact clearly demonstrates that INOY interactions are too soft, resulting in a faster condensation of the nuclear matter. In order to improve the agreement one should try to increase the short-range repulsion between the nucleons. This would inevitably imply a reduction of 3*N* binding energies, although this reduction is not necessarily very large. If one chooses the ITF $^3S_1-{}^3D_1$ and ISA $^1S_0$ potential versions from Ref. [21], which give the smallest probabilities to find nucleons close to each other in 2*N* systems, the resulting triton underbinding will be of only $\sim$50 keV.

Let us finally consider the $n+{}^3$H elastic scattering. This is, in principle, the simplest 4*N* reaction, being almost a pure $\mathcal{T}=1$ isospin state and free of Coulomb interaction. However, its simplicity is only apparent. In fact, $n+{}^3$H is a system with very large neutron excess $[\eta=(N-Z)/A=0.5]$. The only stable nucleus having a neutron excess equally large is ^{8}He. Let us be reminded that the AV18+UIX Hamiltonian faces increasing difficulties when describing neutron-rich nuclei. The more elaborate 3NF model, namely Illinois [6], even though being able to improve the agreement with experimental data, still suffers from similar discrepancies [26]. In addition, the $n+{}^3$H system contains several near-threshold resonances of negative parity (see Fig. 4), which strongly affect the scattering observables near $E_{\text{c.m.}}\approx 3$ MeV. Their internal dynamics is richer than that for bound states and it is not clear that they can be described by using the same recipes as those used for solving the underbinding problem. The description of the $n+{}^3$H cross sections in the resonance region is therefore a very challenging task for nucleon-nucleon interaction models.

We have performed extensive calculations of the $n+{}^3$H scattering states only by using the INOY04 potential. The model dependency of the results was checked at $E_{\text{c.m.}}=0$ and 3 MeV with INOY04′. We present in Table VIII the calculated singlet (a_{0+}) and triplet (a_{1+}) scattering lengths together with the deduced coherent value

$$a_c = \frac{1}{4}(a_{0+} + 3a_{1+}) \tag{16}$$

and the zero-energy cross section

TABLE VIII. $n+{}^3$H singlet ($J^\pi=0^+$), triplet ($J^\pi=1^+$) and coherent scattering lengths (in fm) along with zero-energy cross sections. Different model results are compared with the experimental data.

Potential	a_{0+} (fm)	a_{1+} (fm)	a_c (fm)	σ (fm^2)
INOY04	4.00	3.52	3.64	166.5
INOY04′	4.00	3.52	3.64	166.8
AV18	4.27	3.71	3.85	187.0
AV18+UIX	4.04	3.60	3.71	173.4
Experimental	3.70±0.62	3.70±0.21	3.82±0.07 [39]	170±3[38]
	4.98±0.29	3.13±0.11	3.59±0.02 [40]	
	2.10±0.31	4.05±0.09		
	4.45±0.10	3.32±0.02	3.607±0.017 [41]	

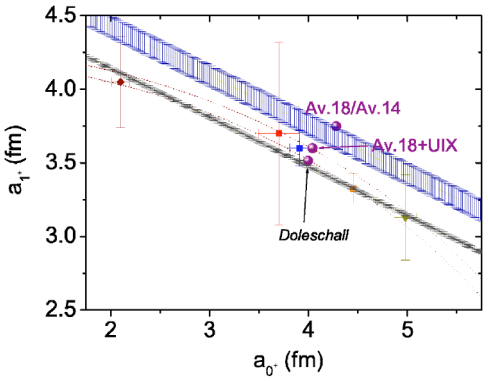

FIG. 5. (Color online) Extraction procedure for $n+{}^3\mathrm{H}$ singlet (a_{0^+}) and triplet (a_{1^+}) scattering lengths from measurements of zero-energy cross section (elliptic band) [38] and coherent scattering length (linear bands) [39–41]. The values of a_i are given by the intersection of these two curves. Bandwidths are related to experimental errors and, even being small, they make their determination very unstable.

$$\sigma(0) = \pi(a_{0+}^2 + 3a_{1+}^2). \tag{17}$$

Results for AV18 and AV18+UIX models have also been obtained and agree at the 1% level with those given in Ref. [35].

The $J^\pi = 0^+$ and 1^+ positive-parity states, determining the low-energy behavior of the $n+{}^3\mathrm{H}$ cross section, do not have any S-matrix singularity, except the triton bound state threshold. It is therefore not surprising that the $n+{}^3\mathrm{H}$ scattering lengths are found to be correlated with $3N$ binding energy, in a similar way as $n+d$ doublet scattering length is Ref. [36]. This is the reason why realistic local interaction models, providing too low $3N$ binding energies, overestimate $n+{}^3\mathrm{H}$ zero-energy cross sections. Once triton binding energy is corrected, for instance by implementing 3NF, a value close to the experimental one is automatically obtained. From Table VIII it can be seen that the Doleschall potential agrees with the lower bound of experimentally measured zero-energy cross section, whereas the AV18+UIX model coincides with its upper bound. The zero-energy scattering cross section is thus fairly well reproduced.

The situation with scattering lengths looks more precarious. The values found in the literature are hardly compatible with each other [37], as can be seen in Table VIII. The usual way to get a_i is to express them in terms of the measured quantities a_c and $\sigma(0)$, by reversing relations (16) and (17). This procedure, represented in Fig. 5, is numerically unstable. Indeed, once $\sigma(0)$ is fixed, the domain of permitted a_{1+} and a_{0+} values is given by the ellipse of Eq. (17) in the (a_{0+}, a_{1+}) plane. Since there are uncertainties in $\sigma(0)$, the permitted values of scattering lengths are trapped in between two ellipsis (dotted curves in Fig. 5). On the other hand, each measurement of a_c restricts a_{1+} and a_{0+} values to lie on a straight line which spreads into a band due to experimental errors (see Fig. 5). The lower band displayed in Fig. 5 follows from the R-matrix analysis result $a_c = 3.607 \pm 0.017$ fm [41], while the upper one comes from the experimental measurement $a_c = 3.82 \pm 0.07$ fm from Ref. [39]. By assuming an exact value of a_c, e.g., $a_c = 3.624$ fm given by the top of the lower band, the present—though small—experimental error in $\sigma(0)$ leads to two sets of solutions which spread over a wide range: (i) $a_{0^+} = [4.31 - 5.00]$, $a_{1^+} = [3.16 - 3.40]$, and (ii) $a_{0^+} = [2.25 - 2.94]$, $a_{1^+} = [3.85 - 4.08]$ fm. This example illustrates the difficulty of extracting reliable values of a_{0^+} and a_{1^+}. The accurate determination of a_i would require us to gain one order of magnitude in measuring both $\sigma(0)$ and a_c.

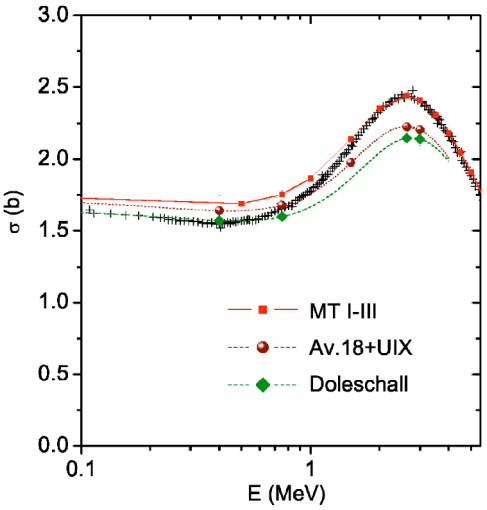

FIG. 6. (Color online) Comparison between experimental and theoretical $n-{}^3\mathrm{H}$ total cross section calculated with several local and nonlocal NN potentials.

As it can be seen also from Fig. 5, the coherent scattering length value $a_c = 3.82 \pm 0.07$ fm of Ref. [39] is in evident disagreement with the experimentally measured zero-energy cross sections, since it does not intersect the $\sigma(0)$ ellipsis. In this respect, the more recent values $a_c = 3.607 \pm 0.017$ fm [41] and $a_c = 3.59 \pm 0.02$ fm [40] are more reliable. The Doleschall nonlocal potential provides $a_c = 3.63$ fm, one standard deviation from these measurements, and seems to be more compatible with data than the AV18+UIX model. Figure 5 suggests also that the real value of the zero-energy cross section should coincide with the lower bound of the experimental result.

The success in describing $n+{}^3\mathrm{H}$ scattering lengths by the Doleschall potential is visible at slightly higher energies as well. In Fig. 6 we present our calculated elastic cross section for the scattering energies in the $n+{}^3\mathrm{H}$ center of mass energy range from 0 to 3 MeV. The Doleschall potential reproduces experimental cross sections near its minima at $E_{\mathrm{c.m.}} \approx 0.4$ MeV. In this region both Malfliet-Tjon (MT) I-III—the only potential known to us being capable to reproduce the resonant region [43]—and AV18+UIX overestimate the experimental value.

In previous works [30,37,42,44,45] we pointed out that local realistic interaction models underestimate the cross sections near the resonance peak, $E_{\mathrm{c.m.}} = 3$ MeV. At that time, calculations had been, however, performed with a limited number of partial waves and the failure was attributed in Ref. [47] to a lack of convergence. Recently we have considerably increased our basis set and have shown that the disagreement is indeed a consequence of nuclear models

TABLE IX. Convergence of $n+t$ scattering lengths and selected phase shifts at $E_{\mathrm{c.m.}}=2.625$ MeV for the INOY04 model. Corresponding mixing parameters are given in parentheses.

j_{yz}	a_0^+ (fm)	a_1^+ (fm)	$\delta(1^+)$ (deg)	$\delta(1^-)$ (deg)
1	3.889	3.609	—	—
2	3.995	3.508	−56.13 −0.757 (0.803)	21.32 39.54 (−42.05)
3	3.995	3.513	−56.12 −0.759 (0.803)	21.39 39.74 (−43.06)
4	3.995	3.515	−56.12 −0.759 (0.803)	21.39 39.76 (−43.16)

[26,46]. The convergence of our present results is shown in Table IX, following the same truncation criteria as for α particles (see Table VII). The number of FY partial amplitudes involved in $n+t$ scattering calculations is considerably larger than for a pure 0^+ bound state and we have not been able to go in the partial wave basis (PWB) as far than in Table VII. One can, however, remark that the results displayed on Table IX converge pretty well, and provide at least three-digit accuracy.

Implementation of 3NF is just able to improve zero-energy cross sections and is not efficient at the resonance energies. Doleschall nonlocal potentials seem to suffer from a similar defect: the phase shifts obtained using INOY04 are even slightly smaller in their absolute value (except for the 2^- state) than those obtained with local potentials and the total cross section is slightly worse. In fact the reduction of positive-parity phase shifts is a consequence of improving triton binding energies. As was previously discussed, $n+{}^3$H scattering lengths are linearly correlated with the triton binding energy. Whichever way one uses to increase triton binding, by means of nonlocal interaction or 3*NF*, the final result will inevitably be a reduction of 0^+ and 1^+ $n+{}^3$H scattering lengths and low-energy phase shifts (in absolute value). It turns out that by the same way, we reduce in absolute value the 0^- and 1^- phase shifts. Only 2^- phases are slightly increased in both AV18+UIX and Doleschall models. Thus we have a real puzzle for the interaction models: on one hand they have to reduce low-energy cross sections, while on the other hand cross sections in the resonance region should be significantly increased. The fact that all realistic interactions systematically suffer in the resonance region lead us to believe that the underlying reason of this disagreement is not related to the nonlocality or to 3NF effects. The observed discrepancies have different background than the underbinding problem. Where does this failure come from?

When analyzing $n+{}^3$H cross sections in the resonance region, one should first recall their origin. They are negative-parity states and their symmetry is consequently different from the positive-parity ones, which are dominated by *S* waves. The good agreement of the scattering lengths provided by the Doleschall potential as well as its success in reproducing the low-energy cross section minima make us believe that the positive-parity phases are quite well reproduced in the resonance region as well. On the other hand, negative-parity phase shifts should be rather far from reality, causing a disagreement with the experimental data.

To understand the possible source of such a disagreement, we have calculated—as for the *nd* case—the relative contribution of the different *NN* partial waves in the integral expression of the phase shifts (12). The obtained results are summarized in Table X. The first two rows correspond to the 0^+ at $E=0$ and $E=3$ MeV. One can see that positive-parity states are completely controlled by the interaction in ${}^3SD_1$ and ${}^1S_0$ waves, at zero energies as well as at $E_{\mathrm{c.m.}}=3$ MeV, close to resonance peak. The role of higher partial waves is marginal. The situation changes dramatically in negative-parity states (values in rows 3–5). The contribution of *P*-wave interactions becomes comparable to the *S* wave. On the other hand, the nontriviality of physics in the resonance region is reflected by the strong compensation of different *P* waves as well as ${}^3D_1$ and ${}^3S_1$ components in the ${}^3SD_1$ channel. In addition, different *P* waves dominate in different states: in 2^- state, the ${}^3P_2$ waves are the most relevant, whereas ${}^3P_0$ is almost negligible; in the 0^- state, the ${}^3P_0$ wave has the largest contribution, while $3P_2$ fades away.

Finally, we would like to comment that all the observables where *NN P* waves are contributing have a tendency to disagree with the experimental data. A small disagreement can already be seen in *n-d* doublet scattering lengths (Table IV), whereas the triton, described by the same quantum numbers but where *P* waves are negligible, is perfectly reproduced. Other examples could be the 3*N* analyzing powers [48,49], as well as the increasing discrepancy when describing binding energies of neutron-rich nuclei (see Fig. 1). One should

TABLE X. Relative contributions of different *NN* interaction waves in $n-{}^3$H integral scattering lengths (second half of the table).

	J^π	$E_{\mathrm{c.m.}}$ (MeV)	${}^1S_0$	${}^3S_1$	${}^1P_1$	${}^3P_0$	${}^3P_1$	${}^3P_2$	${}^1D_2$	${}^3D_1$	${}^3D_2$	${}^3D_3$	Others
INOY04′	0+	0.0	75.95	22.83	3.588	−1.301	1.942	−0.8112	−0.8661	−1.433	0.1145	0.006131	0.0188
INOY04′	0+	3.0	79.79	19.68	3.413	−1.046	1.913	−0.5796	−0.5796	−1.837	0.0745	0.005113	−0.0803
INOY04	0−	3.0	61.93	67.82	−0.3569	32.97	−26.58	2.190	1.897	−40.41	0.6489	−0.6528	0.5551
INOY04′	0−	3.0	64.16	70.14	−0.3769	32.83	−29.71	2.305	1.987	−41.90	0.6723	−0.6919	0.5750
INOY04′	2−	3.0	39.75	54.90	−0.1640	1.063	−6.893	14.29	0.0970	−3.182	0.1476	.0001	0.0092

also recall that *P* waves in most of the *NN* interactions are tuned on *n-p* and *p-p* data. Moreover, *p-p P* waves are overcast by Coulomb repulsion, while *n-n P* waves are not directly controlled by experiment at all. This study suggests that charge symmetry breaking (CSB) and charge independence breaking (CIB) effects can be sizable in *n-n P* waves and provide a possible explanation for the disagreement observed in $n-{}^3\mathrm{H}$ resonance region.

IV. CONCLUSIONS

During the last decade, a series of nonlocal *NN* potentials has been developed by Doleschall and collaborators and were found to provide an overall satisfactory description of the 2*N* and 3*N* system. If they left unsolved some of the theoretical nuclear problems—like the so-called A_y puzzle—they constitute an undoubted success for their ability to reproduce the experimental binding energy of ^{3}H and ^{3}He nuclei without adding three-nucleon forces.

In this work, we have examined the possibilities for these nonlocal potentials to describe the 4*N* system as well. This system is a cornerstone in the nuclear *ab initio* calculations and a crucial test for the nuclear models, not only because therein the underbinding problem manifests in its full strength, but also because of the rich variety of scattering states it possesses.

We have found that nonlocal *NN* models could well provide 3*N* and 4*N* binding energies in agreement with the experimental data without making explicit use of three-nucleon forces. They offer a solution to cope with the nuclear underbinding problem other than the one offered by the local plus 3NF philosophy.

In their present form, they overbind ^{4}He by some 0.7 MeV, a discrepancy much smaller than all the existing models and which reverses the lack of binding observed in most realistic potentials. The fluctuations in the predictions between different versions of the nonlocal models suggest that a finer parametrization of their internal nonlocal part could be enough to make them fully successful in that point. The current version seems to be too soft in the short-range region, thus giving slightly too small rms radii of light nuclei.

By calculating $n+{}^3\mathrm{H}$ scattering states, we have found that Doleschall models are also very encouraging in describing the low-energy parameters, providing an even better description than Nijm II or AV18+UIX. However, they fail also in reproducing the elastic cross section few MeV above, in the resonance region. In a series of preceding works [26,42,44,46] we have shown that local realistic interactions, even implemented with 3NF, underestimate the cross sections at the resonance peak $E_{\mathrm{c.m.}}=3$ MeV. Unfortunately, the nonlocal models do not solve this problem. On the contrary, they even provide slightly smaller values of the cross section. We believe than the reason for this failure is common to all realistic models and lies in the nucleon-nucleon *P* waves themselves. The analysis of their contribution shows that, contrary to ^{4}He binding energy, they play a crucial role in the $n+{}^3\mathrm{H}$ cross sections. If the *n-p P* waves seem to be well controlled by the experimental data, one still has a relative freedom in the *n-n* ones to improve the description.

ACKNOWLEDGMENTS

Numerical calculations were performed at Institut du Développement et des Ressources en Informatique Scientifique (IDRIS) from CNRS and at Centre de Calcul Recherche et Technologie (CCRT) from CEA Bruyères le Châtel. We are grateful to the staff members of these two organizations for their kind hospitality and useful advice.

[1] S. R. Beane, P. F. Bedaque, A. Parreno, M. J. Savage, Phys. Lett. B **585**, 106 (2004).
[2] S. R. Beane, *Plenary talk at 17th International IUPAP Conference on Few-Body Problems in Physics, June, 2003*, Durham, North Carolina [Nucl. Phys. **A737**, 16 (2004)].
[3] Nuclear Physics with Lattice QCD, White Paper Writing Group, http://www-ctp.mit.edu/negele/WhitePaper.pdf.
[4] R. B. Wiringa, V. G. J. Stoks, and R. Schiavilla, Phys. Rev. C **51**, 38 (1995).
[5] V. G. J. Stoks, R. A. M. Klomp, C. P. F. Terheggen, and J. J. de Swart, Phys. Rev. C **49**, 2950 (1994).
[6] S. C. Pieper, V. R. Pandharipande, R. B. Wiringa, and J. Carlson, Phys. Rev. C **64**, 014001 (2001).
[7] K. Varga, S. C. Pieper, Y. Suzuki, and R. B. Wiringa, Phys. Rev. C **66**, 044310 (2002).
[8] A. Nogga, H. Kamada, W. Glöckle, and B. R. Barrett, Phys. Rev. C **65**, 054003 (2002).
[9] J. L. Friar, G. L. Payne, V. G. J. Stoks, and J. J. de Swart, Phys. Lett. B **311**, 4 (1993).
[10] R. Machleidt, Phys. Rev. C **63**, 024001 (2001).
[11] D. R. Entem and R. Machleidt, Phys. Lett. B **524**, 93 (2002).
[12] E. Epelbaum, W. Glöckle, and U. G. Meissner, Nucl. Phys. **A637**, 107 (1998).
[13] E. Epelbaum, W. Glöckle, and U. G. Meissner, Nucl. Phys. **A671**, 295 (2000).
[14] W. Glöckle, W. Polyzou, Few-Body Syst. **89**, 97 (1990).
[15] W. N. Polyzou, Phys. Rev. C **58**, 91 (1998).
[16] A. Stadler and F. Gross, Phys. Rev. Lett. **78**, 26 (1997).
[17] P. Doleschall, Nucl. Phys. **A602**, 60 (1996).
[18] P. Doleschall, Few-Body Syst. **23**, 149 (1998).
[19] P. Doleschall and I. Borbély, Few-Body Syst. **27**, 1 (1999).
[20] P. Doleschall and I. Borbély, Phys. Rev. C **62**, 054004 (2000).
[21] P. Doleschall and I. Borbély, Nucl. Phys. **A684**, 557c (2001).
[22] P. Doleschall, I. Borbély, Z. Papp, and W. Plessas, Phys. Rev. C **67**, 064005 (2003).
[23] P. Doleschall, Phys. Rev. C **69**, 054001 (2004).
[24] A. Amghar and B. Desplanques, Nucl. Phys. **A714**, 502 (2003).
[25] V. I. Kukulin, V. N. Pomerantsev, A. Faessler, A. J. Buchmann, and E. M. Tursunov, Phys. Rev. C **57**, 535 (1998).
[26] R. Lazauskas, Ph.D. thesis, Université Joseph Fourier, Grenoble (2003); http://tel.ccsd.cnrs.fr/documents/archives0/00/00/41/78/
[27] L. D. Faddeev, Zh. Eksp. Teor. Fiz. **39**, 1459 (1960) [Sov.

Phys. JETP **12**, 1014 (1961)].
[28] O. A. Yakubowsky, Sov. J. Nucl. Phys. **5**, 937 (1967).
[29] S. P. Merkuriev and S. L. Yakovlev, Theor. Math. Phys. **56**, 673 (1983).
[30] F. Ciesielski, Ph.D. thesis, Université Joseph Fourier, Grenoble (1997).
[31] B. S. Pudliner, V. R. Pandharipande, J. Carlson, and R. B. Wiringa, Phys. Rev. Lett. **74**, 4396 (1995).
[32] A. Nogga, A. Kievsky, H. Kamada, W. Glöckle, L. E. Marcucci, S. Rosati, and M. Viviani, Phys. Rev. C **67**, 034004 (2003).
[33] P. Doleschall (private communications).
[34] A. Nogga, Ph.D. thesis, Ruhr-Universität, Bochum (2001).
[35] M. Viviani, S. Rosati, and A. Kievsky, Phys. Rev. Lett. **81**, 1580 (1998).
[36] A. C. Philips, Phys. Lett. **28B**, 378 (1969); Rep. Prog. Phys. **40**, 905 (1977).
[37] J. Carbonell, Nucl. Phys. **A684**, 218 (2001).
[38] T. W. Phillips, B. L. Berman, and J. D. Seagrave, Phys. Rev. C **22**, 384 (1980).
[39] S. Hammerschmied, H. Rauch, H. Clerc, and U. Kischko, Z. Phys. A **302**, 323 (1981).
[40] H. Rauch, D. Tuppinger, H. Wolwitsch, T. Wroblewski, Phys. Lett. **165B**, 39 (1985).
[41] G. M. Hale *et al.*, Phys. Rev. C **42**, 438 (1990).
[42] F. Ciesielski, J. Carbonell, and C. Gignoux, Nucl. Phys. **A631**, 653c (1998).
[43] F. Ciesielski and J. Carbonell, Phys. Rev. C **58**, 58 (1998). [We notice a misprint in Table. VIII: a and r_0 for a given S line must be inverted, in agreement with Table VII.]
[44] F. Ciesielski, J. Carbonell, C. Gignoux, Phys. Lett. B **447**, 199 (1999).
[45] J. Carbonell, Few-Body Syst., Suppl. **12**, 439 (2000).
[46] R. Lazauskas and J. Carbonell, Contribution to 17th International IUPAP Conference on Few-Body Problems in Physics, June, 2003, Durham, North Carolina [Nucl. Phys. **A737**, S79 (2004)].
[47] A. C. Fonseca, Phys. Rev. Lett. **83**, 4021 (1999).
[48] H. Witala and W. Glöckle, Nucl. Phys. **A528**, 48 (1991).
[49] W. Tornow, H. Witala, and A. Kievsky, Phys. Rev. C **57**, 555 (1998).